Received: 19 February 2021 | Revised: 10 June 2021 | Accepted: 11 June 2021

DOI: 10.1111/1750-3841.15841

FOOD CHEMISTRY

Journal of Food Science WILEY

Penicillin biosensor based on rhombus-shaped porous carbon/hematoxylin/penicillinase

Hongsu Wang[1] | **Li Wang**[1] | **Yi Xiu**[1] | **Shaoqi Zhang**[1] | **Song Wang**[2] | **Xiaodi Niu**[1]

[1] College of Food Science and Engineering, Jilin University, Changchun, People's Republic of China

[2] Laboratory of Theoretical and Computational Chemistry, Institute of Theoretical Chemistry, Jilin University, Changchun, People's Republic of China

Correspondence
Xiaodi Niu, College of Food Science and Engineering, Jilin University, Changchun 130062, People's Republic of China.
Email: niuxd@jlu.edu.cn

Funding information
Key Program of Jilin Province, Grant/Award Number: 20200402060NC; International Cooperation Project of Science and Technology Department of Jilin Province, Grant/Award Number: 20190701032GH; Science and Technology Project in Jilin Province Department of Education, Grant/Award Number: JJKH20211126KJ; National Nature Science Foundation of China, Grant/Award Number: 31572566

Abstract: In this experiment, we designed an electrochemical sensor using penicillinase (Pen X)-rhombus porous carbon (RPC) as the detection element and hematoxylin as the indicator to detect low concentrations of penicillin sodium (Pen G). A differential pulse voltammetry (DPV) method was used to detect Pen G in the concentration range of 10^{-8}–10^{-5} mg·mL^{-1} under optimal experimental conditions. The results showed that the peak current value and the logarithm of Pen G concentration showed a good linear relationship ($R^2 = 0.9915$), and the LOD was 2.68×10^{-7} mg·mL^{-1} (S/N = 3). The actual milk samples were detected by the addition method and compared with the high-performance liquid phase method; no significant difference was found in the detection results. The working electrode prepared by cross-linking method not only extends the service life of the sensor, but also improves the sensitivity and reproducibility of the sensor. It can also be used to detect the Pen G residue in the actual milk samples repeatedly.

Practical Application: In this study, an electrochemical sensor for the rapid detection of penicillin sodium in milk was prepared, which has good sensitivity and fast detection speed.

KEYWORDS
detection, electrochemical sensor, penicillin sodium, rhombus porous carbon microspheres

1 | INTRODUCTION

β-lactams are a widely used class of antibiotics represented by those containing a β-lactam ring within their molecular structure (Pham et al., 2019). In the treatment of veterinary diseases, Pen G is the most commonly used β-lactam antibiotic for preventing and treating bacterial infections such as cow mastitis (Van Boeckel et al., 2015). Pen G can persist in small amounts, which may cause allergic reactions in sensitized individuals (Jalili et al., 2020). Penicillin residues may also induce drug-resistant bacteria and may negatively affect the growth of fermented dairy products at other levels (Junza et al., 2014).

At present, many practical and effective methods have been adopted to detect β-lactam antibiotics within the food industry and animal husbandry, such as liquid chromatography (HPLC) (Samanidou et al., 2007), liquid chromatography-mass spectrometry (LC-MS) (Kipper et al., 2017), enzyme-linked immunosorbent assay (ELISA) (Font et al., 2008; Zhao et al., 2007), and microbial detection methods (Myllyniemi et al., 2002). However, these methods are time-consuming, expensive, environmentally demanding, and require complex sample preparation (Dey et al., 2005; Gramse & Jacobson, 2005; Picó & Barceló, 2008). Therefore, it is important to develop a fast and reliable method for quantifying Pen G in foods.

Recently, biosensors have become promising alternatives to traditional analysis systems for a variety of applications in environmental monitoring (Khoshbin et al., 2020; Uen et al., 2020; Gupta et al., 2014), food analysis (Li et al., 2018; Sun et al., 2020), and clinical diagnostics (Ehzari et al., 2020; Goyal et al., 2009; Gupta et al., 2015; Zhang & Fan, 2020). In addition, biosensors have low requirements for the detection environment and require minimal sample preparation (Barthelmebs et al., 2010; Xiu et al., 2020). Mesoporous carbon materials have been widely used in electrochemical sensors owing to their attractive properties, including extremely high specific surface area (Qiu et al., 2012; Yang et al., 2020), excellent mechanical stability (Cargnello et al., 2012), and good thermal stability and electrical conductivity (Istamboulie et al., 2017; Zhu & Diao, 2011). Metal-organic frameworks (MOFs) are self-assembled structures that can control the structural morphology and pore size of materials (Liu et al., 2008). The process of carbonizing the MOF material can retain the original structure and the corresponding pore structure. The electrochemical performance mainly depends on the active material, suitable structure, and pore size (Zhang et al., 2014). The results show that micropores can significantly increase the specific surface area of carbon materials, improve the contact site of charge in carbon materials, enhance the storage capacity of charge in supercapacitors, and improve the electrochemical performance (Luo et al., 2018). In this study, an Al-based MOF was used as a precursor to prepare porous carbon. This method has a lower production cost, and the porous carbon material prepared has a new rhombus structure (Jiang et al., 2019), a larger specific surface area, higher thermal stability, and better electrochemical performance than other carbon materials (Salihu et al., 2019).

Under alkaline conditions, hematoxylin (HE) exists in an oxidized state. Pen X can catalyze the β-lactam ring of Pen G to produce penicillic acid (PA) and release H^+ (Wu et al., 2014). With the H^+ concentration increased, the electrons can be obtained from oxidized hematoxylin (O HE), which promotes the reduction of oxidized hematoxylin on the electrode surface. When the operating potential is constant, the current value of the reaction is proportional to the pH value of the system. The reaction is sensitive to the change of H^+ concentration, which is very suitable for the determination of small acidity changes in samples (Fig. S1) (Stred'ansky et al., 2000). Therefore, it can be used for rapid quantitative determination of Pen G.

In this study, a rhombus-shaped porous carbon (RPC) prepared by the template method using an aluminum-based metal organic framework (Al-MOF) as a template was used as a carrier for penicillinase (Pen X). To prepare the conjugate Pen X/RPC, the conjugate was used to modify the electrode to obtain the working electrode Pen X/RPC/GCE, treating HE as an indicator and optimizing the preparation and detection conditions of the working electrode, as shown in Scheme 1. Finally, the DPV method was used to detect the Pen G content, and the stability and uniformity of the prepared electrode were determined. The sensor prepared by cross-linking method not only extends the service life of the sensor, greatly enhances the stability and reproducibility of the sensor, but also uses the RPC as the carrier material to improve the conductivity of the electrode and obtain a more sensitive response signal. By comparing with the traditional method for detecting Pen G, the application of the sensor prepared in this experiment to actual milk samples was explored.

2 | MATERIALS AND METHODS

2.1 | Chemicals and apparatus

Aluminum nitrate ($Al(NO_3)_3{\cdot}9H_2O$), anhydrous ethanol (C_2H_5OH), pyromellitic acid ($C_9H_6O_6$), ammonium persulfate ($(NH_4)_2S_2O_8$), sulfuric acid (H_2SO_4), potassium chloride (KCl), potassium ferricyanide ($K_3[Fe(CN)_6]$), and potassium ferrocyanide ($K_4Fe(CN)_6{\cdot}3H_2O$) were purchased from Xilong Chemical Co., Ltd. Penicillinase and hematoxylin ($C_{16}H_{14}O_6$) were purchased from Shanghai Yuanye Biotechnology Co., Ltd. Penicillin sodium ($C_{16}H_{17}N_2NaO_4S$) was purchased from Sigma-Aldrich and phosphate buffered saline (PBS) was purchased from Yikangda. Milk samples were purchased from a local supermarket.

The physical and chemical properties of the synthesized RPC material were characterized using the following methods. A JEOL S-4800 scanning electron microscope (SEM) was used to characterize the morphology of the two materials under an acceleration voltage of 10 kV and transmission electron microscopy (TEM, Tecnai G2F30) at an operating voltage of 100 kV. Using a D8 Advance X-ray diffractometer (XRD) device equipped with CuKα radiation ($\lambda = 0.154060$ nm) at a scan rate of $2°{\cdot}min^{-1}$ and a range of 2θ from 10° to 80° to analyze the product structure. The RPC materials' surface functional groups were characterized using an IR Prestige-21 Fourier Infrared Spectrometer (IR Prestige-2). The specific surface area and pore size of the RPC material were characterized by N_2 adsorption-desorption isotherms. The instrument used was a Micromeritics ASAP 2020 analyzer. The elemental composition of RPC was determined by X-ray photoelectron spectroscopy (XPS; SSI S-Probex). Simultaneously, for separating the nutrients in milk, we used a TGL-16M high-speed desktop refrigerated centrifuge, the electrochemical signals were measured by CHI660e electrochemical workstation with three electrode system, Ag/AgCl as reference

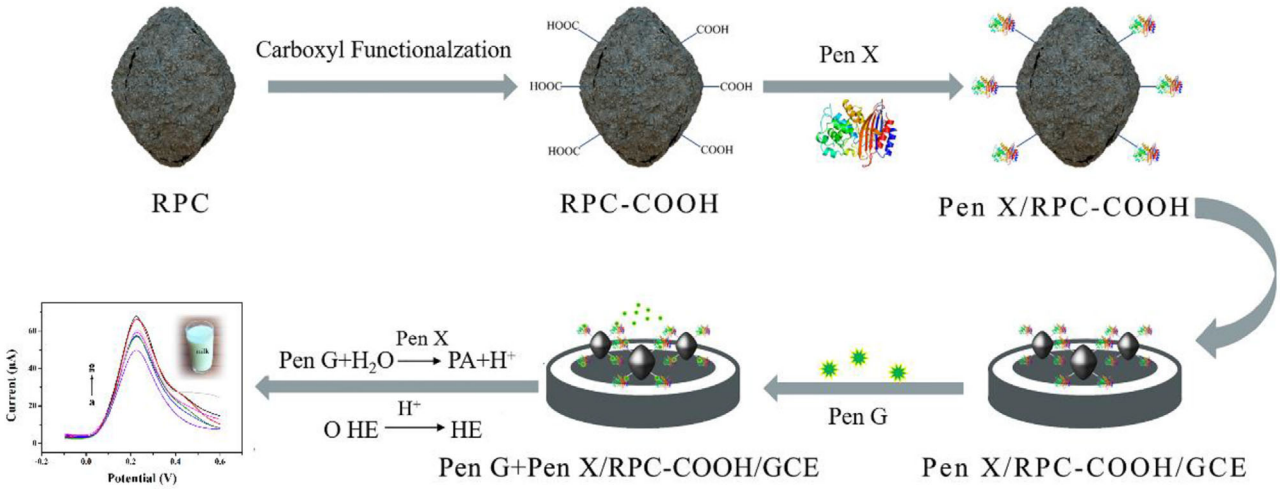

SCHEME 1 Schematic illustration of the preparation of electrochemical sensor based on an RPC for rapid detection of penicillin sodium

electrode and Pt as counter electrode. The measurement methods include CV (voltage range -0.1–0.6 V), differential pulse voltammetry (pulse amplitude 0.05 V, pulse height 0.05 s, interval between pulses 0.5 s, base potential increment 0.004 V), electrochemical impedance spectrum (sinusoidal voltage perturbation 0.005 V, frequency range 1–100000 Hz, and 12 data points per frequency decade).

2.2 | Preparation of RPC

The RPC preparation method was adjusted based on the literature (Jiang et al., 2019). The specific method was as follows: 0.63 g of Al $(NO_3)_3 \cdot 9H_2O$ was added to 25 mL of distilled water and stirred for 20 min. Then, we added 26.6 mL ethanol and 0.56 g trimellitic acid. The solution was stirred for 30 min, and the mixture was poured into a reaction kettle at 120°C for 12 hr. The white powder obtained was centrifuged and washed several times with ethanol and water alternately and dried overnight at 60°C. The sample was placed in a nickel boat by heating in a tube furnace at 5°C·min^{-1} from room temperature to 800°C, maintaining it under N_2 atmosphere for 2 hr for carbonization, and then cooled to 25°C to obtain an RPC sample.

2.3 | Immobilization of penicillinase and determination of enzyme activity

Carboxyl modification of the prepared RPC by the wet oxidation method (Vinu et al., 2007). The specific method is to pour about 300 mg of RPC into 15 mL of 1.75 M $(NH_4)_2S_2O_8$ and 15 mL of 2 M H_2SO_4 mixed solution and mix well. The reaction was carried out at 40°C for 24 hr, the supernatant was discarded by centrifugation, the precipitate was repeatedly washed with deionized water to neutrality, and the carboxyl-modified material RPC-COOH was obtained.

Next, 30 mL of Thris-HCl buffer was added and 5 mg EDC and 6 mg NHS were added to dissolve the solution. Then, a certain amount of carboxyl-functionalized material RPC-COOH was added to the above solution and dispersed for 30 min under ultrasound. Afterwards, 2 mL of Pen X at specific concentrations were added at certain temperatures and different speeds for a period; after centrifugation and repeated washing, the upper washing solution was collected for later determination of Pen X loading. An enzyme-immobilized material was obtained and stored at 4°C. The amount of penicillinase, relative enzyme activity, and immobilized enzyme activity were determined according to the method in the literature (Xiu et al., 2019).

2.4 | Working electrode preparation

5 μL of a certain mass fraction of the solid-loaded material was dropped onto a clean GCE and dried at 4°C to obtain a working electrode. A three-electrode system and DPV method were used to detect a series of penicillin sodium solutions containing a certain amount of hematoxylin in different concentrations.

2.5 | Determination of penicillin sodium in milk samples

Pure milk was purchased from a local supermarket, and 200 mL was measured, adding 60 g of ammonium sulfate for salting out. The samples were centrifuged at 5000 rpm for 20 min at room temperature, and milk samples

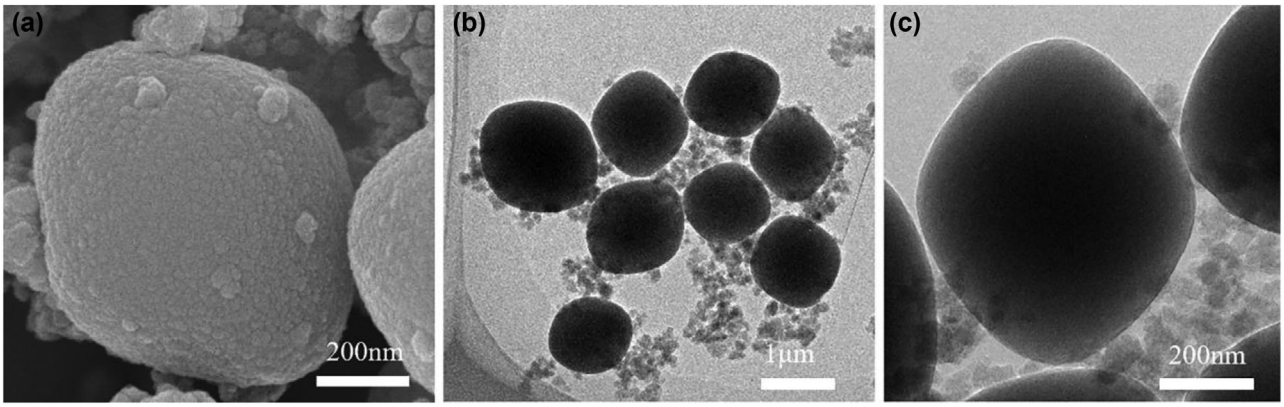

FIGURE 1 SEM (A) and TEM (B,C) of the RPC

were collected by filtration through a sterile microporous membrane (0.22 μm). The pH of the milk sample was adjusted with PBS, and a standard was added for measurement. Simultaneously, the results were compared with HPLC results to confirm the accuracy of the sensor in the detection of reagent samples.

2.6 | Determination of sensor stability and specificity

The working electrode was placed at 4°C and stored for 7 days; then the Pen G test was repeated six times at the same concentration (10^{-5} mg·mL^{-1}). The peak current value was then recorded. After 30 days of storage, the Pen G test was repeated an additional six times at the same concentration to calculate relative standard deviation (RSD).

Under the same conditions, the prepared working electrode was used to detect amoxicillin, cephalexin, and penicillin potassium and compared with the peak current value of penicillin sodium at the same concentration (10^{-2} mg·mL^{-1}).

3 | RESULTS AND DISCUSSION

3.1 | Characterization of RPC

The morphology and structural characteristics of RPC can be observed from the SEM and TEM images. As shown in Figure 1A, many relatively uniform rhombus-shaped porous carbons materials can be found with an average diameter of approximately 500 nm. In addition, the special structure of this rhombus is complete and has good dispersion. This rhombus-shaped structure can also be observed in Figure 1B,C, with uniform size and good dispersibility. It can also prove that this rhombus-shaped porous carbon material was successfully synthesized.

To further prove the successful synthesis of RPC, Figure 2 shows the RPC XRD pattern, FT-IR pattern, and nitrogen adsorption-desorption and BET patterns. From Figure 2A, it can be observed that there are characteristic diffraction peaks at $2\theta = 23°$ and 45°, corresponding to the (002) and (101) crystal planes, respectively (Hu et al., 2018), which are characteristic peaks of carbon materials. The diffraction peak attributed to alumina at $2\theta = 67°$ proves that the synthesized material contains aluminum (Jiang et al., 2019). Therefore, XRD characterization proved that this material was successfully synthesized.

Figure 2B shows the FT-IR diagram of the material. It is observed in the figure that the absorption bands at 740 cm^{-1} and 1379 cm^{-1} correspond to Al-O bonds, and the RPC-COOH after carboxyl functionalization can see the absorption peak of -OH at 3404 cm^{-1}; a C = C peak at 1082 cm^{-1} and the absorption peak at 1790 cm^{-1} represent the formation of C = O bonds (Hu et al., 2018; Liu et al., 2012). This shows that there are carboxyl groups on the surface of the material, proving the successful synthesis of RPC-COOH. Compared with curve b, the peak of -CO-NH appeared at 1531 cm^{-1} in curve c, and the absorption peak of -OH is enhanced at 3404 cm^{-1}, indicating that Pen X is successfully immobilized on the electrode.

As shown in Figure 2C, the nitrogen adsorption isotherm of RPC is a typical IV curve (Zhu & Diao, 2011). Under a higher pressure ($P/P_0 = 0.9$), the sharp rise reflects the existence of a macropore structure, indicating that mesopores are formed in the material. As shown in Figure 2D, the pore size of RPC was mainly distributed at 31 nm, and it can be calculated that the specific surface area of RPC was 100.2424 m^{2}g, and the pore volume was 0.2688 cm^3·g^{-1}, indicating that the material had a certain pore structure.

Figure 3 shows the X-ray photoelectron spectroscopy (XPS) of RPC, showing the elemental composition of RPC and the electronic states of C and Al. Figure 3A indicates that the synthesized material mainly contains

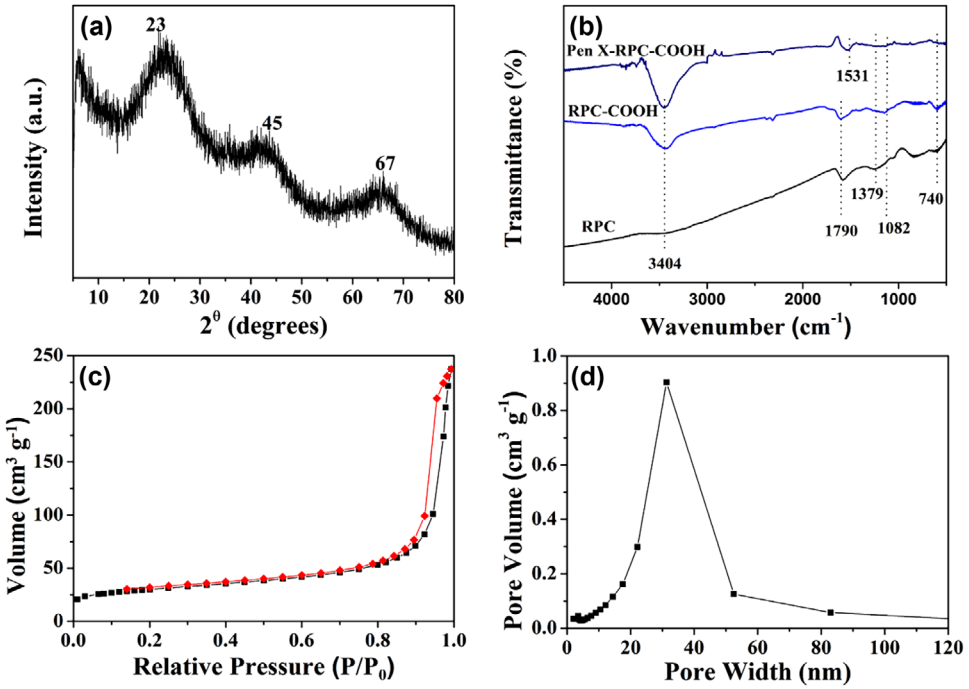

FIGURE 2 (A) X-ray diffraction (XRD) patterns of RPC; (B) Fourier-transform infrared (FT-IR) spectra of RPC, RPC-COOH, Pen X-RPC-GCE; (C,D) nitrogen adsorption-desorption isotherm and BJH pore size distribution curve of RPC

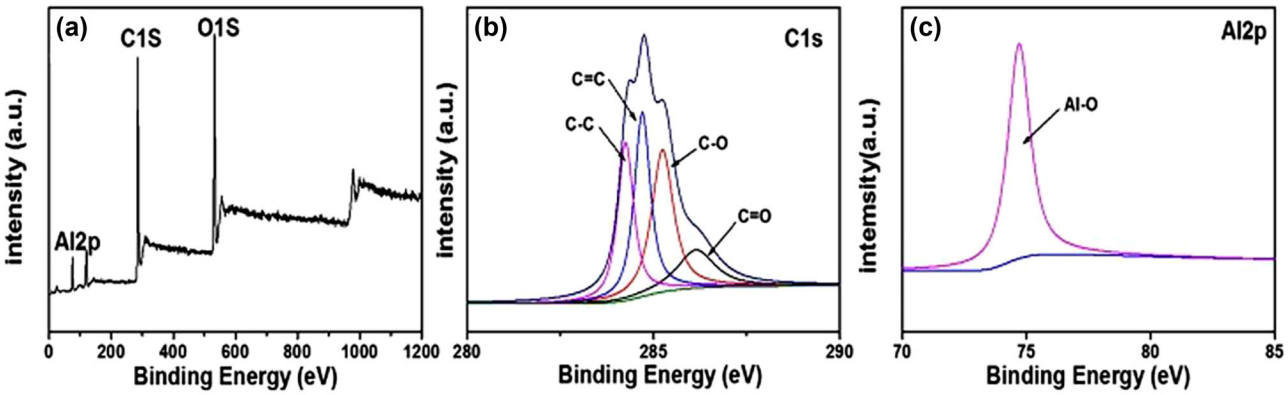

FIGURE 3 XPS map of RPC (A); magnified map of C 1S (B) and Al 2p (C)

three elements C, O, and Al and the peak intensity of Al 2p is relatively weak. At the same time, the high-resolution C 1s spectrum (Figure 3B) shows that the C in RPC is C-C, C = C, C-O, and C = O, and the peak positions correspond to 284.2, 284.6, 285.3, and 287.1 eV, respectively (Liu et al., 2012). Figure 3C shows that the form of Al is Al-O, and the peak position is 74.7 eV (Jiang et al., 2019). Table S1 lists the percentage of each element content; it can be seen that the carbon content is the highest (Sarawade et al., 2014).

3.2 | Electrochemical characterization

In electrochemical analysis, electrochemical impedance spectroscopy (EIS) is a common method. In the Nyquist impedance plot, the semicircle represents the charge transfer resistance (Rct), and the impedance value of the prepared electrode can be calculated according to the radius (Gupta et al., 2015; He et al., 2020). R_S is the solution resistance, Cdl is the constant phase element resistance corresponding to the double-layer capacitor, and W is a Warburg

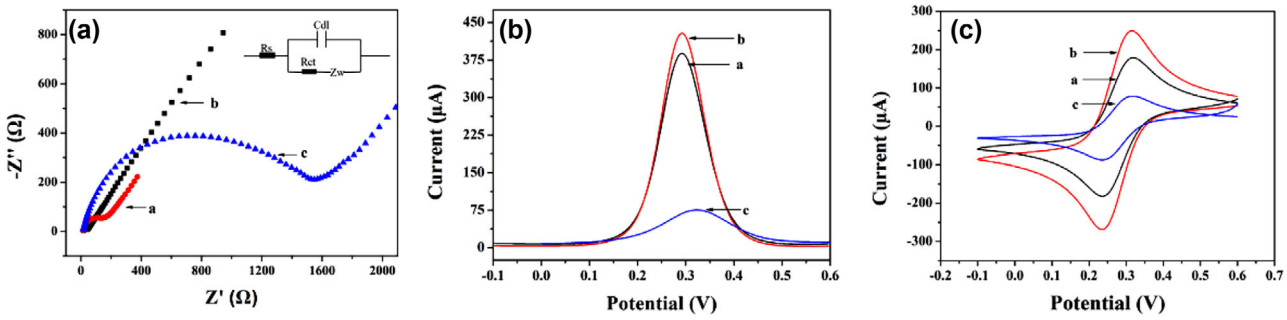

FIGURE 4 EIS (A), DPV (B), and CV (C) in 1 mM $[Fe(CN)_6]^{3-/4-}$ (including 0.1 M KCl) solution for characterization of GCE (a), RPC/GCE (b), and Pen X/RPC/GCE (c)

short circuit term of finite length coupled with Rct (Figure 4A inset). The EIS spectra of GCE (a), RPC/GCE (b) and Pen X/RPC/GCE (c) in 1 mM $[Fe(CN)_6]^{3-/4-}$ (containing 0.1 M KCl) solution and open circuit voltage of 0.24 V are shown in Figure 4A. In the high-frequency region, there is a descending semicircle, followed by a straight line with a slope close to 45°. Compared with bare GCE semicircle, the semicircle diameter of modified RPC electrode decreased significantly, and the semicircle diameter increased significantly after further fixation with Pen X. This may be related to the combination of charge transfer resistance and double-layer capacitance of the electroactive materials on the electrode surface, indicating that the electrode modified by RPC improves the electron transfer rate. However, when the non-conductive Pen X is modified on the electrode, the repulsion between $[Fe(CN)_6]^{3-/4-}$ hinders the electron transfer at the interface, resulting in a high impedance (Farokhi et al., 2020).

Figure 4B shows the differential pulse voltammetry (DPV) curves of different electrodes in 1 mM $[Fe(CN)_6]^{3-/4-}$ solution. It can be seen from the figure that the peak current of the bare electrode is 405 μA. When RPC is fixed on the electrode surface, the peak current significantly increases because RPC increases the conductivity of the electrode. However, when the RPC with Pen X adsorbed was fixed on the electrode surface, the peak current value decreased significantly. This is because the adsorption of Pen X prevents the transfer of electrons on the electrode, thereby reducing the peak current value. This can also prove that the enzyme was successfully immobilized on the material, which was consistent with the results obtained on the EIS.

Cyclic voltammetry (CV) is a commonly used method in electrochemical characterization. Figure 4C shows the CV curves of GCE (a), RPC/GCE (b), and Pen X/RPC/GCE (c). It was observed from curve that GCE has a good redox peak, while curve B has a slightly larger redox peak, which may be because the modification of GCE by RPC with good electron transport capability enhances the electron transfer on the electrode surface. Compared with curves a and b, the redox peak current value of curve c decreases significantly. This may be owing to the non-conduction of Pen X, which hinders the transfer of electrons, resulting in a decrease in the conductivity of the electrode. This also proves that Pen X was successfully modified to the electrode surface. The results obtained from the CV were consistent with the DPV and EIS results.

3.3 | The kinetic analysis of sensor

Figure 5A shows the CV of Pen X/RPC/GCE at different scan rates. The scanning peak current (including the oxidation peak current and reduction peak current) increases as the scan rate increases. Figure 5B shows that there is a good linear relationship between the scanning peak current and the square roots at different scan rate, I/μA = 14.338x + 16.379 (R^2 = 0.9919) and I/μA = −12.360x-37.369 (R^2 = 0.9978). The correlation coefficient was greater than 0.99; the oxidation process follows the adsorption mechanism and diffusion mechanism, mainly adsorption (Joseph, 2006; Shahrokhian et al., 2018; Ye et al., 2021). Through the Randles–Sevick equation (Chokkareddy et al., 2020; Garcia-Miranda Ferrari et al., 2018; Kilele et al., 2020):

$$I_{pa} = 2.69 \times 10^5 A C n^{3/2} {D_R}^{1/2} v^{1/2}$$

where I_{pa} is the peak current of the anode, A is the surface area of the electrode, n is the number of transferred electrons, C is the concentration of the detection solution, D_R is the diffusion coefficient, and v is the scan rate. The results show that the surface area of the working electrode is 27.29 mm^2, while that of the bare electrode is 7.068 mm^2, which indicates that the RPC immobilized on the electrode surface can effectively promote the rapid transfer of

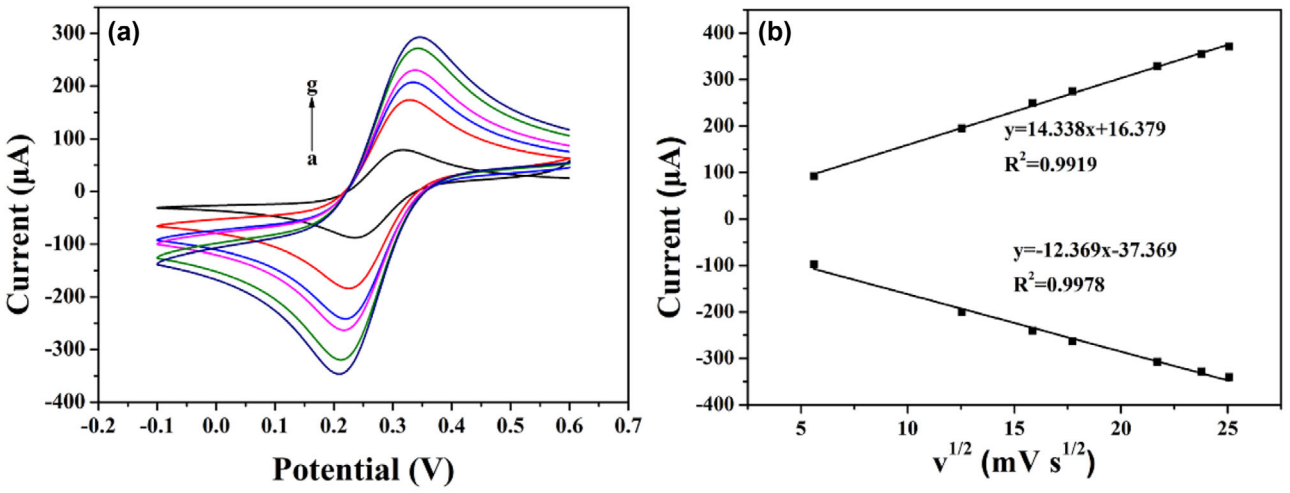

FIGURE 5 (A) CV of Pen X/RPC/GCE at different scanning speeds of 10 (a), 50 (b), 80 (c), 100(d), 150 (e), 180 (f), and 200(g) mV·s^{-1} in 1 mM $[Fe(CN)_6]^{3-/4-}$ (including 0.1 M KCl) and (B) the linear relationship between the square root of the scanning speed and the peak current (values are given as mean ± RSD)

electrons on the electrode surface (Rajasekhar Chokkareddy et al., 2020), and obtain a higher peak current (Figure 4) than that of the bare electrode.

3.4 | Optimization of experimental parameter conditions

To determine the optimal conditions for sensor preparation and reduce the impact on the current value during electrochemical detection, the effects of immobilization time, pH, rotation speed, temperature, carrier mass, and enzyme concentration on immobilization capacity and related enzyme activities were investigated. The optimal immobilized enzyme conditions were obtained by optimizing immobilization conditions: we choose initial enzyme concentration 1 mg·mL^{-1}, temperature 30°C, oscillator revolution 150 rpm, carrier mass 30 mg, immobilization time 2 hr, and pH 6.5 as the optimal loading conditions. Under the optimal loading conditions, the loading capacity of RPC to Pen X was 156 mg·g $^{-1}$, and the relative enzyme activity was 89%. We also explored the detection conditions, choosing 3 mg·mL^{-1} hematoxylin as the best test solution concentration.

3.5 | Detection of penicillin sodium

Using DPV, the oxidation peak current of the Pen X/RPC/GCE electrochemical sensor in solutions of different concentrations of substrate Pen G was measured (as shown in Figured 6A). Based on the measurement results, the relationship between the peak current value and the logarithm of Pen G concentration is plotted in Figured 6B. As shown in Figure 6B, when the Pen G concentration is 10^{-8}-10^{-5} mg·mL^{-1}, the response current of the sensor is linearly related to the logarithm of the Pen G concentration. The linear equation is y = 3.0459x + 66.087 (R^2 = 0.9915), and the calculated detection limit of Pen G by the sensor was 2.68×10^{-7} mg·mL^{-1} (S/N = 3). When the concentration of Pen G gradually increases, the active sites of Pen X on the electrode surface are relatively small, the amount of Pen G adsorption is relatively small, and the current response is relatively small. Therefore, the measured current response has a linear relationship with the logarithm of the concentration, the results are consistent with those in Figure 5. Compared with other studies, as shown in Table 1, the detection limit of the prepared sensor is lower.

3.6 | Detection of milk samples

To prove the actual application of the sensor Pen X/RPC/GCE, we used commercially available milk as a sample, added a certain amount of penicillin sodium using the addition method, and the prepared electrochemical sensor was used to measure and calculate the addition recovery of Pen G rate (Table 2). It was found that the recovery rate of the sensors was close to 100%, indicating that it can be successfully used for the detection of milk samples.

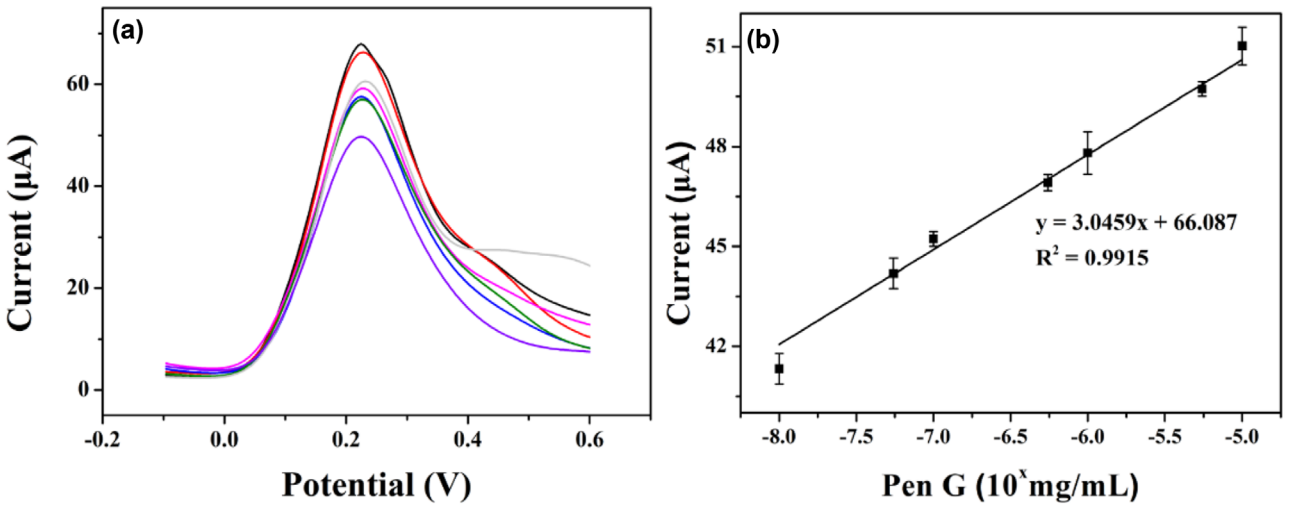

FIGURE 6 (A) DPV of Pen X/RPC/GCE at different concentrations of Pen G; (B) linear relationship between operating current and different Pen G concentrations (values are given as mean ± RSD)

TABLE 1 Comparison of Pen X/RPC/GCE sensors for detection of β-lactam antibiotics

Working electrode	Antibiotic	Detection range	Detection limit	References
MIPs	AMP	1–500 nM	1.89 nM	(Jamieson et al., 2019)
Pen X/Co @ C-PMB-GCE	Pen G	0.27–2.7 and 2.7–27 nM	1.7 nM	(Xiu et al., 2019)
Pen X – NiNPs -SPCE	Pen G	0.01–0.5 M	3.1×10^{5} nM	(Salihu et al., 2019)
anti-CEX/CEX-OVA/ SWNTs-COOH/CS/GCE	CEX	2.88–2303 nM	270 nM	(Yu et al., 2020)
ZnCo / C800-Nafion / GCE	MNZ	50–100000 nM	17 nM	(Baikeli et al., 2020)
QDs-P6LC-PEDOT-PSS/GCE	AMX	900–69000 nM	50 nM	(Wong et al., 2020)
Pen X-RPC-GCE	Pen G	0.028–28 nM	0.75 nM	This work

Note: MIPs, molecularly imprinted polymers; QDs, quantum dots; P6LC, Printex 6L Carbon; PEDOT-PSS: poly (3,4-ethylenedioxythiophene)-poly (styrene sulfonate); AMP, ampicillin sodium; CEX, cephalexin; MNZ, metronidazole; AMX, amoxicillin.

TABLE 2 Comparison of Pen X/RPC/GCE Sensors with high-performance liquid chromatography for the detection of Pen G

Milk sample	Added Pen G ($mg\cdot mL^{-1}$)	Test methods	Found ($mg\cdot mL^{-1}$)	Recovery ± RSD (%) ($n = 3$)
1	10^{-5}	HPLC	1.01×10^{-5} ± 4.78	101 ± 4.78
		Pen X/RPC/GCE	1.06×10^{-5} ± 1.33	106 ± 1.33
2	10^{-6}	HPLC	1.13×10^{-6} ± 4.07	113.4 ± 4.07
		Pen X/RPC/GCE	9.97×10^{-6} ± 1.46	99.7 ± 1.46
3	10^{-7}	HPLC	1.03×10^{-7} ± 3.09	103 ± 3.09
		Pen X/RPC/GCE	1.12×10^{-7} ± 1.08	112 ± 1.08
4	10^{-8}	HPLC	9.1×10^{-8} ± 3.97	91 ± 3.97
		Pen X/RPC/GCE	9.48×10^{-8} ± 1.19	94.8 ± 1.19

TABLE 3 The oxidation peak current in 10^{-8}–10^{-5} mg mL^{-1} penicillin sodium was measured, take the current value at 10^{-5} mg mL^{-1} as an example

Time (day)	Detection Current (μA)	Remained ratio (%)	RSD (%)
0	50.9	100	5.7
7	49.29	96.84	2.2
30	44.27	86.97	6.3

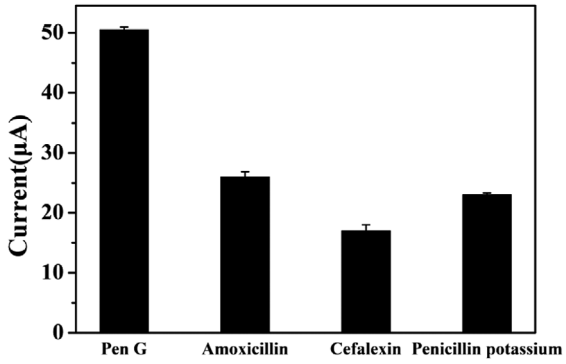

FIGURE 7 Histogram of sensor detecting Pen G, amoxicillin, cefalexin, and penicillin potassium (values are given as mean ± RSD)

3.7 | Accuracy, stability, and specificity testing

Using the working electrode, the measurement was repeated six times in 10^{-5} mg·mL^{-1} penicillin sodium to calculate the accuracy of the electrode. The results show that the relative standard deviation of the electrode is 2.21%, which proves that the accuracy of the electrode is good (Table S3). When the same concentration of penicillin sodium was determined by the same electrode for six times, the current value changed little (RSD = 0.72%), indicating that the prepared electrode had good repeatability (Table S2). Simultaneously, to determine the stability of the sensor, the working electrode was stored at 4°C. The oxidation peak current in 10^{-8}-10^{-5} mg·mL^{-1} penicillin sodium was measured (Table 3), and it was found that the oxidation peak current remained 96.84% of the initial current after 7 days. In addition, the oxidation peak current measured after 30 days retained 86.97% of the initial current, proving that the sensor has good stability.

Under the same conditions, 10^{-2} mg·mL^{-1} amoxicillin, cephalexin, and penicillin potassium were detected with the prepared working electrode and compared with the peak current value of penicillin sodium at the same concentration. Figure 7 indicates that under the same detection conditions, the response current of penicillin sodium is the largest, while the response current values of the other three antibiotics are all smaller. This indicates that the sensor has better specificity.

4 | CONCLUSION

In this study, we studied a rhombus-shaped porous carbon material (RPC) based on an aluminum-based metal organic framework as an electrochemical sensor template and fixed Pen X by a common bond method to obtain Pen X/RPC immobilized enzyme material, which is a new type of Pen G sensing platform. The working electrode Pen X/RPC/GCE was prepared under the optimal loading conditions for the detection of Pen G at different concentrations. It was found that the sensor showed good linearity when the concentration range of Pen G was 10^{-8}-10^{-5} mg·mL^{-1}, with the formula $y = 3.0459x + 66.087$ ($R^2 = 0.9915$). After calculation, the detection limit of Pen G concentration by the sensor was 2.68×10^{-7} mg·mL^{-1} (S/N = 3). In addition, the stability, precision and specificity of the prepared sensor were investigated, and the results proved that the sensor has the advantages of low detection limit, high sensitivity, excellent stability, and the working electrode can be repeatedly used. Using the standard addition method to detect Pen G in milk as an actual sample, the results are satisfactory, indicating that the sensor can be successfully applied for the detection of actual sample milk.

AUTHOR CONTRIBUTIONS

Wang Hongsu and Niu Xiaodi: Formal analysis, methodology, writing-review, and editing. Wang Li and Xiu Yi: Date curation and writing-original draft. Zhang Shaoqi and Wang song: Investigation and visualization.

CONFLICTS OF INTEREST

All authors declare that they have no conflict of interests.

ETHICAL APPROVAL

This article does not contain any studies with human participants or animals performed by any of the authors.

ORCID

Hongsu Wang https://orcid.org/0000-0002-6696-9303

REFERENCES

Baikeli, Y., Mamat, X., Wumaer, M., Muhetaer, M., Aisa, H. A., & Hu, G. (2020). Electrochemical determination of metronidazole using

a glassy carbon electrode modified with nanoporous bimetallic carbon derived from a ZnCo-based metal-organic framework. *Journal of The Electrochemical Society*, *167*(11), 116513. https://doi.org/10.1149/1945-7111/ab9d94

Barthelmebs, L., Calas-Blanchard, C., Istamboulie, G., Marty, J.-L., & Noguer, T. (2010). Biosensors as analytical tools in food fermentation industry. In M. T. Giardi, G. Rea, & B. Berra (Eds.), *Bio-farms for nutraceuticals: Functional food and safety control by biosensors* (Vol. *698*, pp. 293–307). Springer.

Cargnello, M., Grzelczak, M., Rodriguez-Gonzalez, B., Syrgiannis, Z., Bakhmutsky, K., La Parola, V., & Fornasiero, P. (2012). Multiwalled carbon nanotubes drive the activity of metal@oxide core-shell catalysts in modular nanocomposites. *Journal of the American Chemical Society*, *134*(28), 11760–11766. https://doi.org/10.1021/ja304398b

Chokkareddy, R., Kanchi, S., & Inamuddin. (2020). Simultaneous detection of ethambutol and pyrazinamide with IL@$CoFe_2O_4$NPs@MWCNTs fabricated glassy carbon electrode. *Science Report*, *10*(1), 13563. https://doi.org/10.1038/s41598-020-70263-z

Chokkareddy, R., Thondavada, N., Kabane, B., & Redhi, G. G. (2020). A novel ionic liquid based electrochemical sensor for detection of pyrazinamide. *Journal of the Iranian Chemical Society*, *18*(3), 621–629. https://doi.org/10.1007/s13738-020-02047-1

Dey, B. P., Thaker, N. H., Bright, S. A., & Thaler, A. M. (2005). Fast antimicrobial screen test (FAST): Improved screen test for detecting antimicrobial residues in meat tissue. *Journal of Aoac International*, *88*(2), 447–454.

Ehzari, H., Amiri, M., & Safari, M. (2020). Enzyme-free sandwich-type electrochemical immunosensor for highly sensitive prostate specific antigen based on conjugation of quantum dots and antibody on surface of modified glassy carbon electrode with core-shell magnetic metal-organic frameworks. *Talanta*, *210*, 120641. https://doi.org/10.1016/j.talanta.2019.120641

Farokhi, S., Roushani, M., & Hosseini, H. (2020). Design of an electrochemical aptasensor based on porous nickel-cobalt phosphide nanodiscs for the impedimetric determination of ractopamine. *Journal of Electroanalytical Chemistry*, *877*, 114557. https://doi.org/10.1016/j.jelechem.2020.114557

Font, H., Adrian, J., Galve, R., Esevez, M. C., Castellari, M., Gratacos-Cubarsi, M., & Marcot, M. P. (2008). Immunochemical assays for direct sulfonamide antibiotic detection in milk and hair samples using antibody derivatized magnetic nanoparticles. *Journal of Agricultural and Food Chemistry*, *56*(3), 736–743. https://doi.org/10.1021/jf072550n

Garcia-Miranda Ferrari, A., Foster, C. W., Kelly, P. J., Brownson, D. A. C., & Banks, C. E. (2018). Determination of the electrochemical area of screen-printed electrochemical sensing platforms. *Biosensors (Basel)*, *8*(2), 53. https://doi.org/10.3390/bios8020053

Goyal, R. N., Gupta, V. K., & Chatterjee, S. (2009). Fullerene-C_{60}-modified edge plane pyrolytic graphite electrode for the determination of dexamethasone in pharmaceutical formulations and human biological fluids. *Biosensors and Bioelectronics*, *24*(6), 1649–1654. https://doi.org/10.1016/j.bios.2008.08.024

Gramse, M., & Jacobson, P. E. (2005). Determination of penicillin G in feeds by liquid chromatography with solid-phase extraction. *Journal of Aoac International*, *88*(3), 679–683.

Gupta, V. K., Karimi-Maleh, H., & Sadegh, R. (2015). Simultaneous determination of hydroxylamine, phenol and sulfite in water and waste water samples using a voltammetric nanosensor. *International Journal of Electrochemical Science*, *10*(1), 303–316.

Gupta, V. K., Mergu, N., Kumawat, L. K., & Singh, A. K. (2015). A reversible fluorescence "off-on-off" sensor for sequential detection of aluminum and acetate/fluoride ions. *Talanta*, *144*, 80–89. https://doi.org/10.1016/j.talanta.2015.05.053

Gupta, V. K., Singh, A. K., & Kumawat, L. K. (2014). Thiazole Schiff base turn-on fluorescent chemosensor for Al3+ ion. *Sensors and Actuators B: Chemical*, *195*, 98–108. https://doi.org/10.1016/j.snb.2013.12.092

He, H., Wang, S. Q., Han, Z. Y., Tian, X. H., Zhang, W. W., Li, C. P., & Du, M. (2020). Construction of electrochemical aptasensors with Ag(I) metal−organic frameworks toward high-efficient detection of ultra-trace penicillin. *Applied Surface Science*, *531*, 147342. https://doi.org/10.1016/j.apsusc.2020.147342

Hu, Y., Chen, Y., Liu, Y., Li, W., Zhu, M., Hu, P., & Li, Y. (2018). Accordion-like nanoporous carbon derived from Al-MOF as advanced anode material for sodium ion batteries. *Microporous and Mesoporous Materials*, *270*, 67–74. https://doi.org/10.1016/j.micromeso.2018.04.046

Istamboulie, N. P. G., Triki, A., Lozano, C., Barthelmebs, L., & Noguer, T. (2017). Selection of DNA aptamers against penicillin G using capture-SELEX for the development of an impedimetric sensor. *Talanta*, *162*, 232–240. https://doi.org/10.1016/j.talanta.2016.09.058

Jalili, R., Khataee, A., Rashidi, M.-R., & Razmjou, A. (2020). Detection of penicillin G residues in milk based on dual-emission carbon dots and molecularly imprinted polymers. *Food Chemistry*, *314*. https://doi.org/10.1016/j.foodchem.2020.126172

Jamieson, O., Soares, T. C. C., De Faria, B. A., Hudson, A., Mecozzi, F., Rowley-Neale, S., Banks, C. E., Gruber, J., Novakovic, K., Peeters, M., & Crapnell, R. (2019). Screen printed electrode based detection systems for the antibiotic amoxicillin in aqueous samples utilising molecularly imprinted polymers as synthetic receptors. *Chemosensors*, *8*(1), 5. https://doi.org/10.3390/chemosensors8010005

Jiang, W., Pan, J., Wang, J., Cai, J., Gang, X., Liu, X., & Sun, Y. (2019). A coin like porous carbon derived from Al-MOF with enhanced hierarchical structure for fast charging and super long cycle energy storage. *Carbon*, *154*, 428–438. https://doi.org/10.1016/j.carbon.2019.08.035

Joseph, W. (2006). *Analytical electrochemistry*. John Wiley & Sons.

Junza, A., Montane, A., Barbosa, J., Minguillon, C., & Barron, D. (2014). High resolution mass spectrometry in the identification of transformation products and metabolites from beta-lactam antibiotics in thermally treated milk. *Journal of Chromatography A*, *1368*, 89–99. https://doi.org/10.1016/j.chroma.2014.09.056

Khoshbin, Z., Housaindokht, M. R., & Verdian, A. (2020). A low-cost paper-based aptasensor for simultaneous trace-level monitoring of mercury (II) and silver (I) ions. *Analytical Biochemistry*, *597*, 113689. https://doi.org/10.1016/j.ab.2020.113689

Kilele, J. C., Chokkareddy, R., Rono, N., & Redhi, G. G. (2020). A novel electrochemical sensor for selective determination of theophylline in pharmaceutical formulations. *Journal of the Taiwan Institute of Chemical Engineers*, *111*, 228–238. https://doi.org/10.1016/j.jtice.2020.05.007

Kipper, K., Lillenberg, M., Herodes, K., Nei, L., & Haiba, E. (2017). Simultaneous determination of fluoroquinolones and

sulfonamides originating from sewage sludge compost. *ScientificWorldJournal*, *2017*, 9254072. https://doi.org/10.1155/2017/9254072

Li, F., Wang, X., Sun, X., & Guo, Y. (2018). Multiplex electrochemical aptasensor for detecting multiple antibiotics residues based on carbon fiber and mesoporous carbon-gold nanoparticles. *Sensors and Actuators B: Chemical*, *265*, 217–226. https://doi.org/10.1016/j.snb.2018.03.042

Liu, B., Shioyama, H., Akita, T., & Xu, Q. (2008). Metal-organic framework as a template for porous carbon synthesis. *Journal of the American Chemical Society*, *130*(16), 5390. https://doi.org/10.1021/ja7106146

Liu, C., Shih, K., Gao, Y., Li, F., & Wei, L. (2012). Dechlorinating transformation of propachlor through nucleophilic substitution by dithionite on the surface of alumina. *Journal of Soils and Sediments*, *12*(5), 724–733. https://doi.org/10.1007/s11368-012-0506-0

Luo, R., Feng, Z., Shen, G., Xiu, Y., Zhou, Y., Niu, X., & Wang, H. (2018). Acetylcholinesterase biosensor based on mesoporous hollow carbon spheres/core-shell magnetic nanoparticles-modified electrode for the detection of organophosphorus pesticides. *Sensors (Basel)*, *18*(12), 4429. https://doi.org/10.3390/s18124429

Myllyniemi, A. L., Sipila, H., Nuotio, L., Niemi, A., & Honkanen-Buzalski, T. (2002). An indirect conductimetric screening method for the detection of antibiotic residues in bovine kidneys. *Analyst*, *127*(9), 1247–1251. https://doi.org/10.1039/b204175h

Pham, T. V., Mai, X. L., Le, T. A. T., Lee, J. Y., Lee, G., Kim, D. J., & Kim, K. H. (2019). Development and validation of an HPLC method using a less hazardous mobile phase for the determination of some β-Lactams. *Bulletin of the Korean Chemical Society*, *40*(9), 863–871. https://doi.org/10.1002/bkcs.11836

Picó, Y., & Barceló, D. (2008). The expanding role of LC-MS in analyzing metabolites and degradation products of food contaminants. *TrAC Trends in Analytical Chemistry*, *27*(10), 821–835. https://doi.org/10.1016/j.trac.2008.08.009

Qiu, L., Liu, J. Z., Chang, S. L. Y., Wu, Y. Z., & Li, D. (2012). Biomimetic superelastic graphene-based cellular monoliths. *Nature Communications*, *3*, 1241. https://ARTN.124110.1038/ncomms2251

Salihu, S., Yusof, N. A., Mohammad, F., Abdullah, J., & Al-Lohedan, H. A. (2019). Nickel nanoparticle-modified electrode for the electrochemical sensory detection of penicillin G in bovine milk samples. *Journal of Nanomaterials*, *2019*, 1784154. https://doi.org/10.1155/2019/1784154

Samanidou, V. F., Nisyriou, S. A., & Papadoyannis, I. N. (2007). Residue analysis of penicillins in food products of animal origin by HPLC: A review. *Journal of Liquid Chromatography & Related Technologies*, *30*(9-10), 1145–1204. https://doi.org/10.1080/10826070701274320

Sarawade, P., Tan, H., Anjum, D., Cha, D., & Polshettiwar, V. (2014). Size- and shape-controlled synthesis of hexagonal bipyramidal crystals and hollow self-assembled Al-MOF spheres. *Chemsuschem*, *7*(2), 529–535. https://doi.org/10.1002/cssc.201300836

Shahrokhian, S., Shamloofard, M., & Salimian, R. (2018). Investigation of the electrochemical behavior of tizanidine on the surface of glassy carbon electrode modified with multi-walled carbon nanotube/titan yellow–doped polypyrrole. *Journal of Electroanalytical Chemistry*, *823*, 146–154. https://doi.org/10.1016/j.jelechem.2018.06.005

Stred'ansky, M., Pizzariello, A., Stred'anska, S., & Miertus, S. (2000). Amperometric pH-sensing biosensors for urea, penicillin, and oxalacetate. *Analytica Chimica Acta*, *415*(1-2), 151–157. https://doi.org/10.1016/s0003-2670(00)00869-2

Sun, C., Liao, X., Huang, P., Shan, G., Ma, X., Fu, L., & Kong, W. (2020). A self-assembled electrochemical immunosensor for ultrasensitive detection of ochratoxin a in medicinal and edible malt. *Food Chemistry*, *315*, 126289. https://doi.org/10.1016/j.foodchem.2020.126289

Uen, T., Kushiro, K., Hibino, H., & Takai, M. (2020). Surface functionalization of carbon-based sensors with biocompatible polymer to enable electrochemical measurement in protein-rich environment. *Sensors and Actuators B: Chemical*, *309*, 127758. https://doi.org/10.1016/j.snb.2020.127758

Van Boeckel, T. P., Brower, C., Gilbert, M., Grenfell, B. T., Levin, S. A., Robinson, T. P., & Laxminarayan, R. (2015). Global trends in antimicrobial use in food animals. *Proceedings of the National Academy of Sciences of the United States of America*, *112*(18), 5649–5654. https://doi.org/10.1073/pnas.1503141112

Vinu, A., Hossian, K. Z., Srinivasu, P., Miyahara, M., Anandan, S., Gokulakrishnan, N., & Balasubramanian, V. V. (2007). Carboxy-mesoporous carbon and its excellent adsorption capability for proteins. *Journal of Materials Chemistry*, *17*, 1819–1825. https://doi.org/10.1039/b613899c

Wong, A., Santos, A. M., Cincotto, F. H., Moraes, F. C., Fatibello-Filho, O., & Sotomayor, M. (2020). A new electrochemical platform based on low cost nanomaterials for sensitive detection of the amoxicillin antibiotic in different matrices. *Talanta*, *206*, 120252. https://doi.org/10.1016/j.talanta.2019.120252

Wu, Y. T., Tang, L. L., Huang, L. H., Han, Z. Z., Wang, J., & Pan, H. B. (2014). A low detection limit penicillin biosensor based on single graphene nanosheets preadsorbed with hematein/ionic liquids/penicillinase. *Materials Science & Engineering C-Materials for Biological Applications*, *39*, 92–99. https://doi.org/10.1016/j.msec.2014.02.012

Xiu, Y., Luo, R., Han, B., Liu, L., & Wang, H. (2020). Biosensor based on new delhi metal-β-Lactamase-1 for electrochemical determination of penicillin in milk. *Journal of The Electrochemical Society*, *167*(6), 067525. https://doi.org/10.1149/1945-7111/ab8365

Xiu, Y., Luo, R. P., Han, B. Q., Liu, L., & Wang, H. S. (2019). Construction of Co@C hybrid nanostructure: electrochemical biosensor for detection of penicillin sodium in milk. *Food Analytical Methods*, *13*(3), 617–628. https://doi.org/10.1007/s12161-019-01677-3

Yang, H., Sun, X., Zhu, H., Yu, Y., Zhu, Q., Fu, Z., & Zhang, Q. (2020). Nano-porous carbon materials derived from different biomasses for high performance supercapacitors. *Ceramics International*, *46*(5), 5811–5820. https://doi.org/10.1016/j.ceramint.2019.11.031

Ye, C., Chen, X., Zhang, D., Xu, J., Xi, H., Wu, T., & Huang, G. (2021). Study on the properties and reaction mechanism of polypyrrole@norfloxacin molecularly imprinted electrochemical sensor based on three-dimensional CoFe-MOFs/AuNPs. *Electrochimica Acta*, *379*, 138174. https://doi.org/10.1016/j.electacta.2021.138174

Yu, W., Sang, Y., Wang, T., Liu, W., & Wang, X. (2020). Electrochemical immunosensor based on carboxylated single-walled carbon nanotube-chitosan functional layer for the detection of cephalexin. *Food Science and Nutrition*, *8*(2), 1001–1011. https://doi.org/10.1002/fsn3.1382

Zhang, L., Su, Z., Jiang, F., Yang, L., Qian, J., Zhou, Y., & Hong, M. (2014). Highly graphitized nitrogen-doped porous carbon nanopolyhedra derived from ZIF-8 nanocrystals as efficient

electrocatalysts for oxygen reduction reactions. *Nanoscale*, *6*(12), 6590–6602. https://doi.org/10.1039/c4nr00348a

Zhang, R., & Fan, Z. (2020). Nitrogen-doped carbon quantum dots as a "turn off-on" fluorescence sensor based on the redox reaction mechanism for the sensitive detection of dopamine and alpha lipoic acid. *Journal of Photochemistry and Photobiology a-Chemistry*, *392*, 112438. https://doi.org/10.1016/j.jphotochem.2020.112438

Zhao, C., Liu, W., Ling, H., Lu, S., Zhang, Y., Liu, J., & Xi, R. (2007). Preparation of anti-gatifloxacin antibody and development of an indirect competitive enzyme-linked immunosorbent assay for the detection of gatifloxacin residue in milk. *Journal of Agricultural and Food Chemistry*, *55*(17), 6879–6884. https://doi.org/10.1021/jf070978g

Zhu, M. Y., & Diao, G. W. (2011). Review on the progress in synthesis and application of magnetic carbon nanocomposites. *Nanoscale*, *3*(7), 2748–2767. https://doi.org/10.1039/c1nr10165j

SUPPORTING INFORMATION

Additional supporting information may be found online in the Supporting Information section at the end of the article.

How to cite this article: Wang, H., Wang, L., Xiu, Y., Zhang, S., Wang, S., & Niu, X. Penicillin biosensor based on rhombus-shaped porous carbon/hematoxylin/penicillinase. *J Food Sci*. 2021;1–12. https://doi.org/10.1111/1750-3841.15841